Molecular Dynamic Simulation Model for the Growth of Thin Films in The Structure Zone Model

H. Savaloni[*]
Physics Department, University of Tehran, North-Kargar Avenue, Tehran, Iran
Email: savaloni@Khayam.ut.ac.ir / Savaloni@Yahoo.com
S. M. Afzali
Physics Department, University of Arak, Sardasht, Arak, Iran
Mehran Gholipour Shahraki
Physics Department, University of Arak, Sardasht, Arak, Iran

Abstract

A two dimensional molecular dynamic (atomistic) simulation model was used to investigate the relationship between the nano-structure and the deposition parameters; namely, substrate temperature, deposition rate, angle of incidence, surface roughness. Qualitative agreements with the predictions of the structure zone model (SZM) and the theoretical results of Srolovitze and coworkers (1988), as well as expectations through changes in the activated processes during film growth due to changes in deposition parameters (Grovenor and coworkers (1984)) are obtained. It is shown that by enhancing the atomic mobility (i.e., increasing the substrate temperature or/and lowering the deposition rate) films of higher density with fewer voids are produced. By increasing the deposition angle, the nano-structure of the film changes from a dense film with few voids, to a nano-structure with columns/boundless inclined with the same angle (β) towards the incidence atoms with elongated voids. The angle β increases with increasing the deposition angle (α), and in agreement with the tangent rule (Dirks and Leamy (1977)). The angle of bundles (or the angle of the formation of the voids between atomic bundles), and columnar structure are caused by shadowing effects. Results showed that β decreases slowly with increasing surface mobility (i.e., increasing the substrate temperature or/and reducing the deposition rate).

In general, the model provides almost all predicted results and agrees well with observations.

Keywords: Molecular Dynamic; Structure Zone Model; substrate temperature; deposition rate; angle of incidence.

1. Introduction

Thin crystalline and amorphous films are produced or "grown" by vapor deposition onto a substrate by means of PVD, CVD, MBE and etc. During the process of thin film production, various nano-structure characteristics appear which depend on different parameters, such as substrate temperature, angle of incidence "shadowing effect", adatom migration on the substrate surface "surface diffusion", deposition rate, substrate material/roughness and

---

[*] Corresponding author

residual gases [1-7]. All of these deposition parameters play an important role in determining the nano-structure and physical properties of PVD grown films, such as textured surfaces of Si and Ge for solar absorption[8] and optical data storage[9], magnetic anisotropy[10], and a-Si:H for photovoltaics[11].

The most important and commonly reported structure consist of columns of different density material. It is well known now that this density and the grain size directly depend on the substrate temperature [2-5,12,13]. The columnar structure was first reported by Movchan and Demcheshin[12] who examined thick films of metal oxides and proposed a three zone model depending on the reduced temperature (T_s/T_m) (T_s and T_m are the substrate temperature and the melting point of the evaporant, respectively). Thornton[13] included the additional parameter of sputtering pressure which resulted in a further transition zone (Zone T) appearing between Zone I and Zone II. Messier et al[2] reported a revised SZM, using SEM, TEM and FIM, in which evolutionary growth development of physical structure, column/void sizes are assigned as five sub-zones with sizes: 1-3, 5-20, 20-40, 50-200, and 200-400 nm. This shows that each level of physical structure is about a factor of 3 larger than the previous level. Further Messier[14] in an attempt to quantify morphology of thin films at low adatom mobility, proposed a fractal model that results from natural clustering during random ballistic aggregation of atoms. Kaiser[15] reviewed the fundamentals of thin film growth.

Three different zones appear at: $T_s < 0.3 < T_m$, $0.3T_m < T_s < 0.45T_m$, and $T_s > 0.45T_m$ with the following structures: tapered crystallites with domed tops and voids between them, columnar with smooth surface, equiaxed grains or "re-crystallized grain structure" with bright surface, respectively. It should be noted that the values given above may not apply to all materials. The transition temperatures are given as 0.3 T_m and 0.45 T_m, but can vary from 0.22 to 0.3 T_m and 0.45 to 0.5 T_m depending on the materials, compositions and thickness[2-7,14-20]. The dependence of the nano-structure on the deposition rate is reported by Savaloni et al.[4,6], in which an interrelation between deposition rate and substrate temperature is emphasized. The porous structure at substrate temperatures below o.3T_m becomes increasingly more obvious as the deposition angle becomes larger.

Many authors have investigated the zone model structure of different materials[2-7,12, 18,21,22] and found that the tapered crystallites in zone I are composed of a porous columnar network, that increase in size with temperature. From the theoretical or simulation point of view this structure may be related to the shadowing effect which is based on the principle that the peaks receive a greater deposition flux than the valleys. Thus instead of the surface growing at a uniform rate, the peaks grow at a faster rate than the valleys leading to the development of the structure seen in zone I region[23]. The validity of this theory may appear questionable. It could be argued that the deposited atoms can only occupy a finite number of positions (assuming they maintain some sort of regular structure). Dirks and Leamy[1] in their hard disk atomistic simulation of thin film growth, and Messier and Yehoda[22] describing the shadowing effect as "natural clustering due to ballistic aggregation" concluded that the low adatom mobility in zone I can lead to self-shadowing which results in the microstructure of tapered "columnar" morphology with micro-voids. Thus the shadowing effect undoubtedly plays a significant part in the growth of columnar crystals in thin films. When the vapor is deposited by sputtering the shadowing effect is even more pronounced[24,25]. As substrate temperature increases a second mechanism known as surface diffusion is activated. The growth of grains in the structure is attributed to this surface diffusion of atoms. In the two dimensional surface of the film, atoms are able to move around and can diffuse across grain boundaries from one grain to another. Increasing the substrate temperature increases the activation energy of the surface atoms hence the rate of surface diffusion increases[5].

Srolovitz[26] suggested that one driving force for diffusion is grain boundary curvature. In the same paper, he describes what he calls secondary grain growth. Grains which have their atoms arranged in different crystallographic orientations will also have different surface energies. The effect of atom mobility caused by thermally activated hopping processes is modeled by Muller[27,28]. It was found that from a certain substrate temperature onwards the migration rate of adatoms to shadowed regions is large enough to surpass the rate of void incorporation during growth, resulting in a sudden structural change at the transition temperature from a porous columnar structure to a film with no micro-voids.

Computer simulation of thin film growth is of great significance and has attracted the attention of many researchers in recent years. It can be used to replace the analytical solution of theoretical equations to provide a better understanding of the growth mechanism. Many important parameters and effects can be easily studied from the simulation while they may prove to be experimentally difficult. Most of the simulation models can be categorized into either analytic or atomistic[27-35]. The atomistic models normally result in simulated 2D film nano-structure and morphology. Some 3D atomistic deposition models have been reported[35] generating various film solid fractions ranging from 0.128 to 0.582. However, data are rare and some structural readjustments in the models are artificial.

In the present paper, we employ the molecular dynamics simulation method to investigate the effects of deposition conditions; namely, substrate temperature, deposition rate, angle of incidence, roughness of the substrate surface in both normal and oblique incidence, on the nano-structure of a growing film.

2.The model

A two dimensional simulation cell of 640 x 480 pexiel within the XY-plane was considered. The X direction is parallel to the substrate surface. In order to apply the periodic boundary condition two more cells were considered, each at one side of the simulation cell. In simulation of thin films with periodic boundary condition (for infinite system), it is only required to consider these two cells. The Y direction is perpendicular to the substrate surface and free boundary conditions are employed on the +Y surface. The substrate atoms were arranged in two ordered raws of atoms at the bottom of the simulation cell. In the model proposed here, we consider the two-dimensional structure to represent one face of the basic three-dimensional crystallographic unit cells.

Four parameters of X, Y, V_X and V_Y were designated to each atom and an initial value was given to each parameter. The substrate atoms were taken to be fixed at their sites. The number of atoms in each layer is $n = 80$, and with a distance of a (lattice constant) from each other. The height of first layer is taken to be zero, hence the second layer stands at a height of $a\sqrt{3}/2$. The incident (vapor) atoms are produced at a height of $5a$ from the highest atom in the top layer. This was applied, to reduce the simulation time. These atoms move towards the substrate with respect to the deposition angle and the initial velocity which is defined according to the source temperature and the Maxwell Boltzeman distribution. In order to apply the periodic boundary condition, it is sufficient to produce an atom with the same height, velocity and direction in the opposite side of the simulation cell, when an atom moves out from any side of the simulation cell. The migration of the atoms is considered to be uniform until they have not reached the substrate/film, since it is assumed that they do not perform any interaction with each other. However, by approaching to the atomic layer and crossing the cut off radius, their movement is perturbed by the forces applied to them.

The potential energy of the system was expressed as a sum over all pairs of atoms using the classical Lenard-Jones pair potential;

$$u(r_{ij}) = \varepsilon \left[\left(\frac{r_0}{r_{ij}} \right)^{12} - \left(\frac{r_0}{r_{ij}} \right)^{6} \right] \qquad (1)$$

where $u(r_{ij})$ is the interaction energy between atoms i and j separated by distance r_{ij} and ε scales the strength of the interaction and r_0 is a characteristic length of the potential. The values of ε and r_0 for Ni are 0.74 eV and 0.249 nm, respectively. The force is given by;

$$f_k = \frac{48}{r_{ij}^2} \left(\frac{1}{r_{ij}^{12}} - \frac{1}{2r_{ij}^6} \right) \qquad (2)$$

The cut off radius is taken to be equal to $3a$. Therefore, when an atom is reached to a distance of $3a$ of another atom, suddenly a large force is applied on it. In order to avoid this problem a displacement in the potential as;

$$u = u(r) - u(3a) \qquad (3)$$

was implemented. After calculation of the force, new position and velocity for the next time interval is calculated, using the previous position and velocity. At this stage the atom continues to move with the use of a loop in which the force and co-ordinations of the particle/atom is calculated. This movement may prolong until it collides with a surface atom or it goes under the process of few hops before its collision to a surface atom. The adatom may diffuse on the surface according to the diffusion length given by[36];

$$\overline{X} = \frac{1}{2} a_h \left(\frac{\tau_m}{\tau_h} \right)^{1/2} \qquad (4)$$

$$\text{where} \qquad \tau_m = \frac{a_d}{r}; \qquad \tau_h = \frac{1}{\upsilon} \exp\left(\frac{Q_{dif}}{K_B T_s} \right)$$

where τ_m is the deposition time for the growth of one atomic layer and τ_h is the mean time between hops which is determined by the substrate temperature, T_s. a_d is average distance between atoms in the direction perpendicular to the substrate surface (which for a film with bulk density will be close to the lattice spacing), r is the deposition rate, υ is the lattice vibration frequency of the order of $10^{(14)}$ s^{-1}, Q_{dif} is the surface activation energy, and K_B is the Boltzman constant, until it relaxes in one of the potentially preferred sites on the surface.

After completion of the film growth, the packing density of the grown film was calculated according to the procedure described below (figures 1 (a-c)).

The total length of the simulation cell was divided into equal intervals figure 1 (a). In each interval the height of the highest adatom was determined, and was used to produce figures 1(b and c), which is an indication of the film surface. The area under this surface is then calculated and the packing density was obtained from;

$$PD = \frac{A \times n}{S} \qquad (5)$$

where, S is the area under the surface, n is the number of adatoms and A is the area that an adatom can occupy in a film free of any fault.

The model is programmed in C^{++} and is summarized in a flow chart given in figure 2.

Creation of simulation cell and arrangement of atoms are simulated in step 1. In step 2 according to height of layer, new atoms generate. In step 3 the total forces that are applied on the atom are calculated. In step 4 the new co-ordinates of the atom are calculated using the forces obtained in step 3. In step 5, According to the new co-ordinates of the atom the positions of its neighbors were investigated. In Step 6 adatom relax to its preferred site according to diffusion distance or return to step 3.

3. Results and discussion

The films considered were n = 80 atomic sites wide and 700 or 1000 atoms were deposited in all simulations (figures (3-10)). Flat substrates are represented by first two ordered atomic mono-layers, and by distinct peak or a hole in case of rough surface (for investigation of the shadowing effect in both normal and oblique incidence). In order to simulate an infinite system, periodic boundary conditions are applied.

3.1 normal incidence on flat surfaces, as a function of substrate temperature and deposition rate

Figures 3-6 (a-e) show simulation results of Ni films. In figures 3 and 4 the substrate temperature is kept constant at 400 and 1000 K, respectively, while the deposition rate is the variable parameter.

The deposition rates in figures 3 are R = 0.1, 0.3, 0.4 and 0.5 MLs^{-1}, and in figures 4 this is chosen at higher values R = 1, 1.5, 3 and 5 MLs^{-1}.

In figures 5 and 6 the deposition rate is fixed at o.5 and 1 MLs^{-1}, respectively, and the variable parameter is the substrate temperature, which ranges from 400 to 1000 K. These four figures provide a good set of data for our investigation of the influence of substrate temperature and deposition rate on the structure of the grown films.

At low temperatures and deposition rates (e.g., figure 3 (a)), and high temperatures and relatively low deposition rates (e.g., figure 4 (a)) a dense structure is observed, almost without a significant amount of voids. In the first case the structure obtained is due to the domination of the low deposition rate, which provides the necessary time lapse between arriving atoms on the surface, hence the adatom can move on the surface and go under the process of coalescence and produce a packed structure, while in the latter case the high substrate temperature is the dominant parameter and increases the surface diffusion. Increasing the deposition rate in both low and high substrate temperatures (i.e., 400 and 1000 K) leads to porous structure in which holes or voids form between the bundles/columns. This effect is more pronounced in figures 4 (b-d) when compared with figures 3 (b-d), which is due to higher deposition rates that are about 10 times more than that in figures 3. These high rates of deposition cause the adatoms become buried under the following atoms and form structures such as seen in figures 4 (b-d). The origin of this rate-dependent growth behaviour at different temperatures can be attributed to the exponential dependence of the rate of surface diffusion on temperature.

The packing density of two sets of data in figures 3 (a-d) and 4 (a-d) are given in figures 3 (e) and 4 (e), respectively. Both figures show a decrease in film density with increasing the deposition rate, while this decrease happens with higher rate for films in figures 4, in which the deposition rate is much higher than that in figures 3, as discussed above.

The direct influence of substrate temperature is investigated in figures 5 (a-d) and 6 (a-d) with two deposition rates of 0.5 and 1 MLs^{-1}, respectively. At low substrate temperature (i.e., 400 K), again a columnar structure with voids between them is obtained, showing low

mobility of the adatoms (figures 5 (a) and 6 (a)), with low density that is less for higher rate of 1 MLs^{-1} due to increased number of buried adatoms. By increasing the substrate temperature, as expected the diffusion processes dominates other processes (figures 5(b-d) and 6 (b-d)) and higher density films are produced as it is shown in figures 5(e) and 6(e), as is experimentally observed the microstructure of the film changes from porous or columnar to densely packed or re-crystallite films without micro-voids (particularly, more pronounced for lower deposition rates). The onset of the increase in packing density in figures 5 (e) and 6 (e) is about 450 and 550 K (corresponding to $T_s/T_m \sim$ 0.26 and 0.32; about Zone I to Zone II boundary), respectively, where the void fraction starts to decrease in films due to diffusion process, and reach the maximum value of unity at about 850 and 950 K (corresponding to $T_s/T_m \sim$ 0.5 and 0.55; just past the Zone II to Zone III boundary), where the columns in film structure starts to re-crystallize. Both of these temperatures, are consistent with the predictions of SZM[2,3,5,22] and what is expected from the processes occurring during the film growth, according to the changes in activation energies described by Grovenor et al.[3] and Savaloni et al.[4,7].

3.2 *oblique incidence on flat and rough surface*s

In section 1 (introduction), the influence of the substrate temperature on the nano-structure of the growing films in terms of Structure Zone Model (SZM) was discussed. In zone I, where the substrate temperature is below approximately 0.3 T$_m$, the films tend to exhibit a very porous columnar structure. This porous structure becomes more obvious when the deposition angle of adatoms becomes larger (enhances the shadowing effect). Experimental results suggest that the angle of orientation of these columns (relative to the substrate normal) β, in these structures (zone I), is generally smaller than the deposition angle (relative to the substrate normal) α: i.e., the columnar structure is oriented more nearly perpendicular to the substrate than the deposition flux. Dirks and Leamy [1] showed that the columns in these structures obeyed the so called tangent rule;

$$\tan \beta = \frac{1}{2} \tan \alpha. \qquad (4)$$

This relation had been observed empirically by Nieuwenhuizen and Haanstra[37], and being for deposition angles $\alpha \leq 60°$ [1,21]. In addition, Dirks and Leamy[1] and Paudya et al[38] observed that by decreasing the deposition angles and/or increasing the substrate temperature the film density increases.

Different models have discussed the processes involved in oblique evaporation [1,37,39-41]. It is found that surface diffusion plays an important role, particularly with regard to the difference between random and directional surface diffusion.

The latter is induced by the oblique evaporation process. Typical results of our angle calculation from many simulated films is summarized in figures 7 (a-d) and 8 (a-d), for two different substrate temperatures and two deposition rates (i.e., 400 K ($T_s/T_m \sim$ 0.23) and 0.3 MLs^{-1} and 600 K ($T_s/T_m \sim$ 0.35) and 0.5 MLs^{-1}).

Figures 7(a-d), show the results of 400 K substrate temperature in which the angle of the growth of bundles is increasingly inclined towards the incidence atoms, while this is less clear for higher substrate temperature of 600 K (figures 8 (a-d)), particularly at lower deposition angles of 30° and 45°. However, an agreement with the tangent rule is obtained up to 60° deposition angle.

This change in the angle of columns from $T_s = 400$ K to 600 K and obviously at higher substrate temperatures is due to enhanced surface diffusion process, that causes a change in the mechanism of film growth. Hence, as expected by increasing the substrate temperature the surface diffusion dominates the shadowing effect. As the deposition angle increases, the film nano-structure changes from a dense film, with few voids, to a structure in which nearly collinear tracks of elongated voids form and, finally, to a highly porous structure of well formed columns. This is also confirmed in figures 7 (e) and 8 (e) that show the packing density of films grown in figures 7 (a-d) and 8 (a-d).

The competition between shadowing effect due to substrate roughness (high and low points (holes/trenches) on substrate surface) as well as angle of incidence and the surface diffusion effect due to increased substrate temperature can also be observed in figures 9(a-c) and 10 (a-c). In figures 9 (a-b) Ni films are simulated on a surface with one protruding peak on the surface, with a deposition rate of 0.5 MLs^{-1}, for deposition angle of 60 and two substrate temperatures of 800 K ($T_s/T_m \sim 0.46$) and 400 K ($T_s/T_m \sim 0.23$), respectively.

The comparison of these two figures, clearly indicates that at low substrate temperature it is the shadowing effect that is dominant on the surface diffusion, while at higher temperature of 800 K this domination effect has started to reverse. In normal deposition angle, figure 9 (c) (R=0.3 MLs^{-1} and $T_s/T_m \sim$0.58), due to increased surface diffusion, film with zone III structure is resulted, which grows faster on top of the irregularity/peak than that on the smooth section of the surface, consistent with the shadowing theory proposed by Srolovitz et al[26].

In order to examine the extension of this procedure, we produced substrates with a square hole/trench and the films were grown on these substrates under different deposition conditions.

Typical results are shown in figures 10 (a-c). Both figures 10 (a) and 10 (b) are grown at the same substrate temperature of 400 K, while the deposition rate in these figures is 0.7 MLs^{-1} and 0.3 MLs^{-1}, respectively. Again on the smooth section of the surface in both figures, one can observe the effect of deposition rate on the structure of the grown film, as a result of increased diffusion in lower deposition rate. Around the hole/trench it can be seen that after deposition of a few monolayers, the entrance of the hole/trench is closed and then the film grows on top of these monolayers, almost similar to the other parts of the substrate surface, hence the growing film forgets about its initial stage/state. Similar features are observed in figure 10 (c) ($T_s = 800$ K, R = 0.3 MLs^{-1}) to that of figure 10 (b) ($T_s = 400$ K, R = 0.3 MLs^{-1}), except that due to increased temperature in figure 10 (c) the diffusion rate is increased and the expected structure of zone III is resulted with lesser number/density of voids.

The results presented here are again in qualitative agreement with both experiment, although in much smaller scale and with theoretical predictions.

1. Conclusions

A two dimensional molecular dynamic (atomistic) simulation model was used to investigate the relationship between the nan0-structure and the deposition parameters; namely, substrate temperature, deposition rate, angle of incidence, surface roughness. Qualitative agreements with the predictions of the structure zone model (SZM) and the theoretical results of Srolovitze[26], as well as expectations through changes in the activated processes during film growth due to changes in deposition parameters[3] obtained. It is shown that by enhancing the atomic mobility (i.e., increasing the substrate temperature or/and lowering the deposition rate) films of higher density with fewer voids are produced. By increasing the deposition angle, the structure of film changes from a dense film with few voids, to a structure with

columns/boundless inclined with the same angle (β) towards the incidence atoms with elongated voids. The angle β increases with increasing the deposition angle (α), and in agreement with the tangent rule [1]. The angle of bundles (or the angle of the formation of the voids between atomic bundles), are caused by shadowing effects.

In general, the model provides almost all predicted results and agrees well with observations.

Acknowledgements
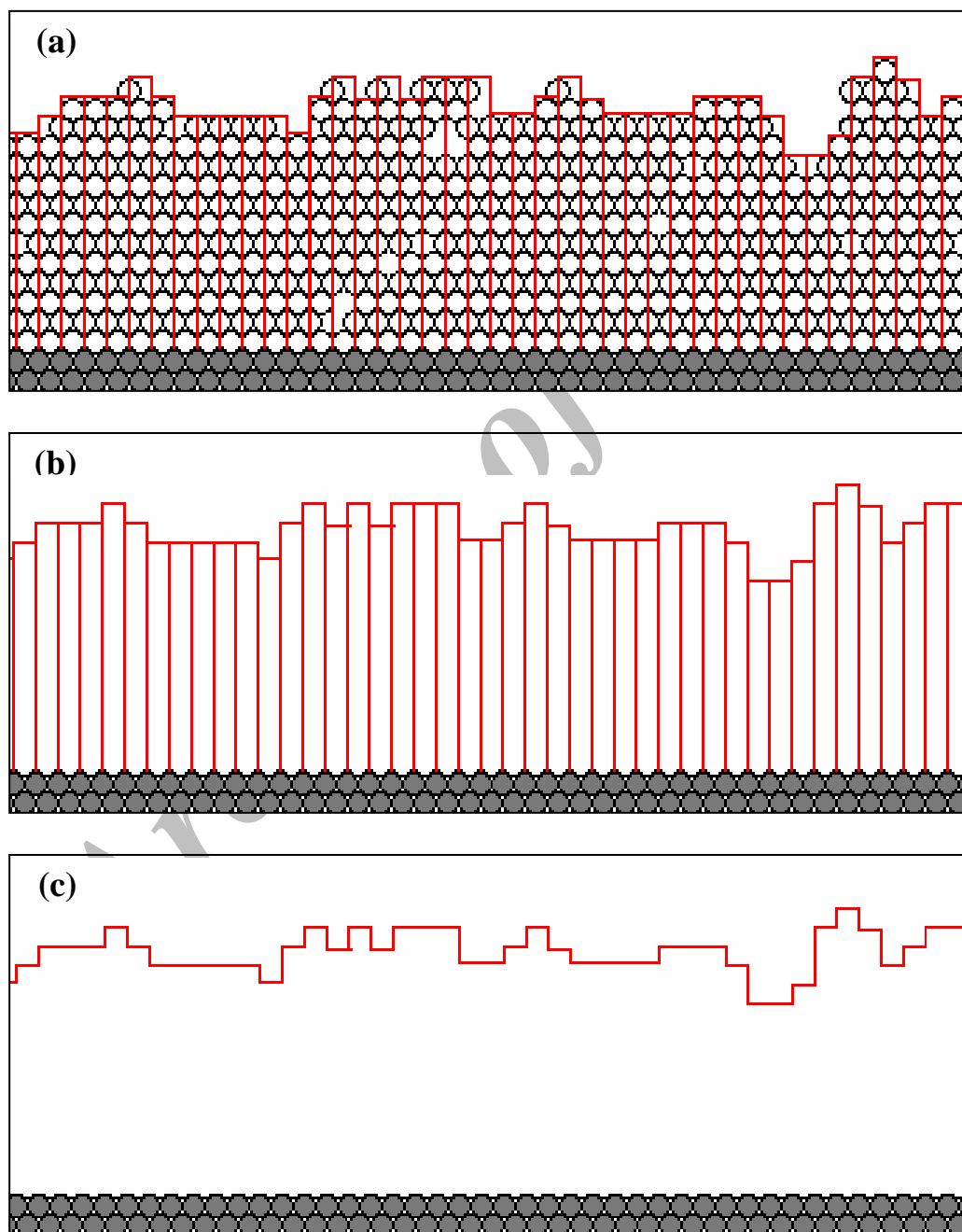
Figure 1. Procedure of calculation of packing density of grown film. a) A typical grown film; total length of simulation cell is divided into equal intervals.
b and c) the surface of the film and the area under the film surface is determined, respectively

```
┌─────────────────────────────┐
│  Creation of simulation cells │
└─────────────────────────────┘
              │
              ▼
┌─────────────────────────────┐
│      Generate a new atom      │◄────────┐
└─────────────────────────────┘         │
              │                          │
              ▼                          │
┌─────────────────────────────┐         │
│   Calculation of total forces │         │
└─────────────────────────────┘         │
              │                          │
              ▼                          │
┌─────────────────────────────┐         │
│  Calculation of new cordinates│         │
└─────────────────────────────┘         │
              │                          │
              ▼                          │
┌─────────────────────────────┐         │
│   Investigation of neighbors  │         │
└─────────────────────────────┘         │
              │                          │
  ┌─────┐     ▼          ┌─────┐         │
  │ No  │◄─ Relaxation ─►│ Yes │─────────┘
  └─────┘                └─────┘
```
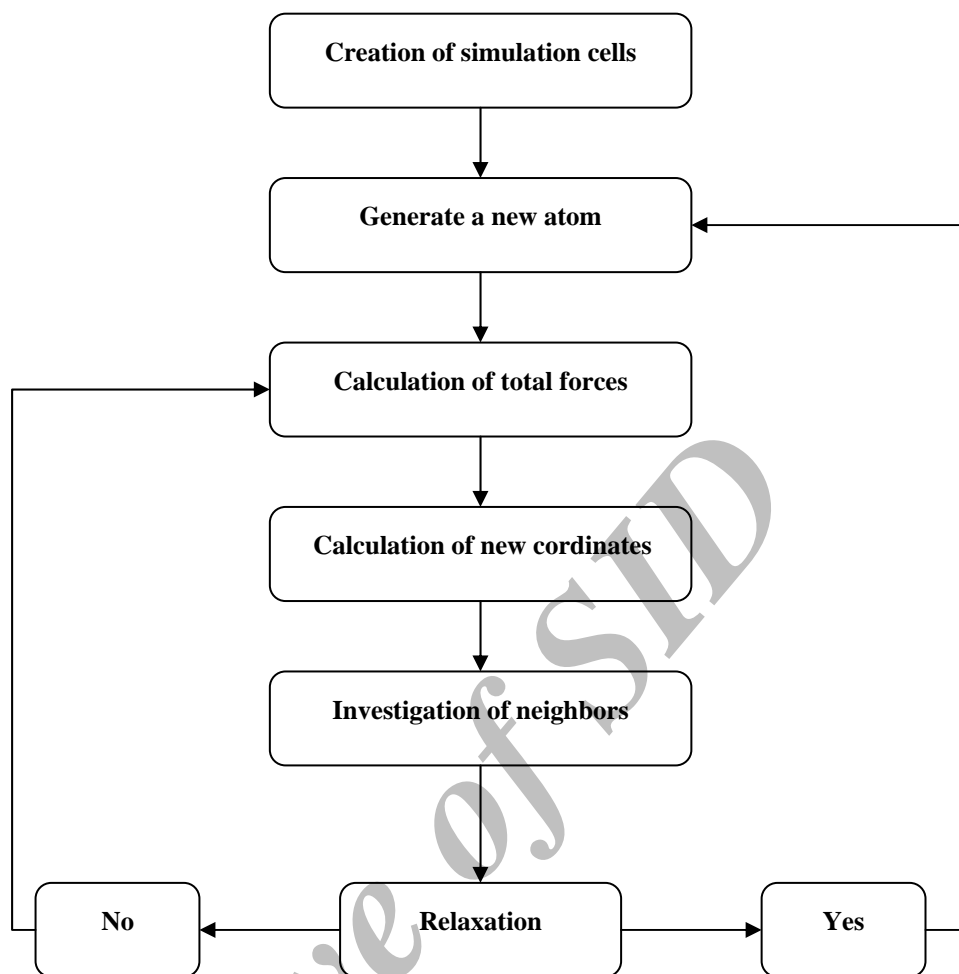
Figure 2. Flowchart of the algorithm for the deposition of a layer.

(b)

(d)
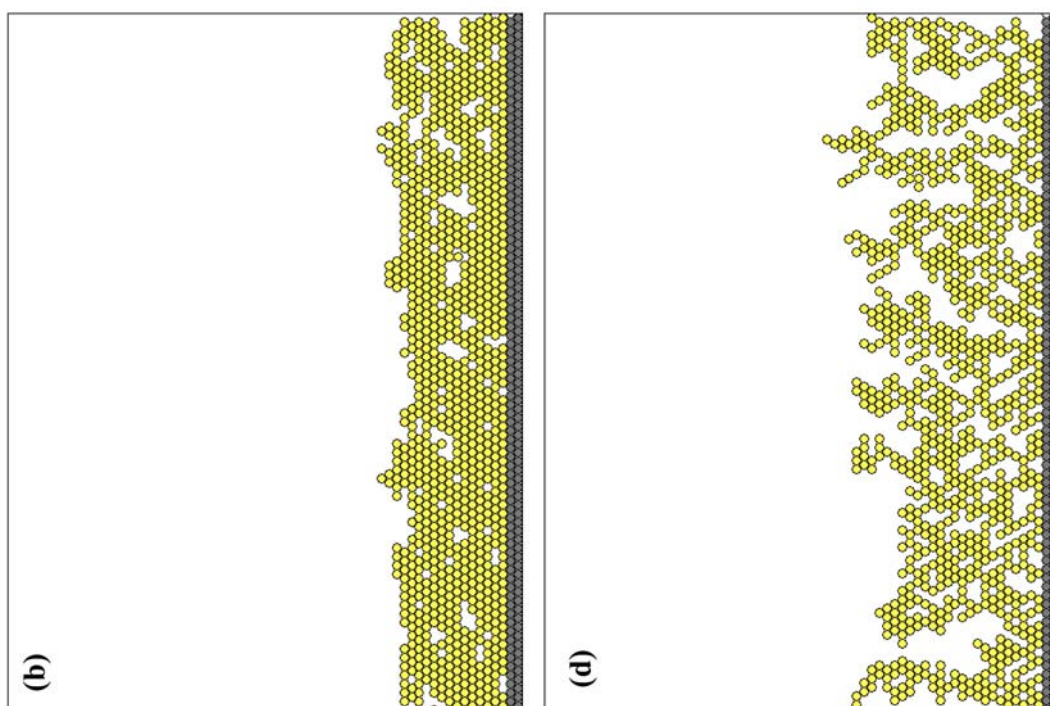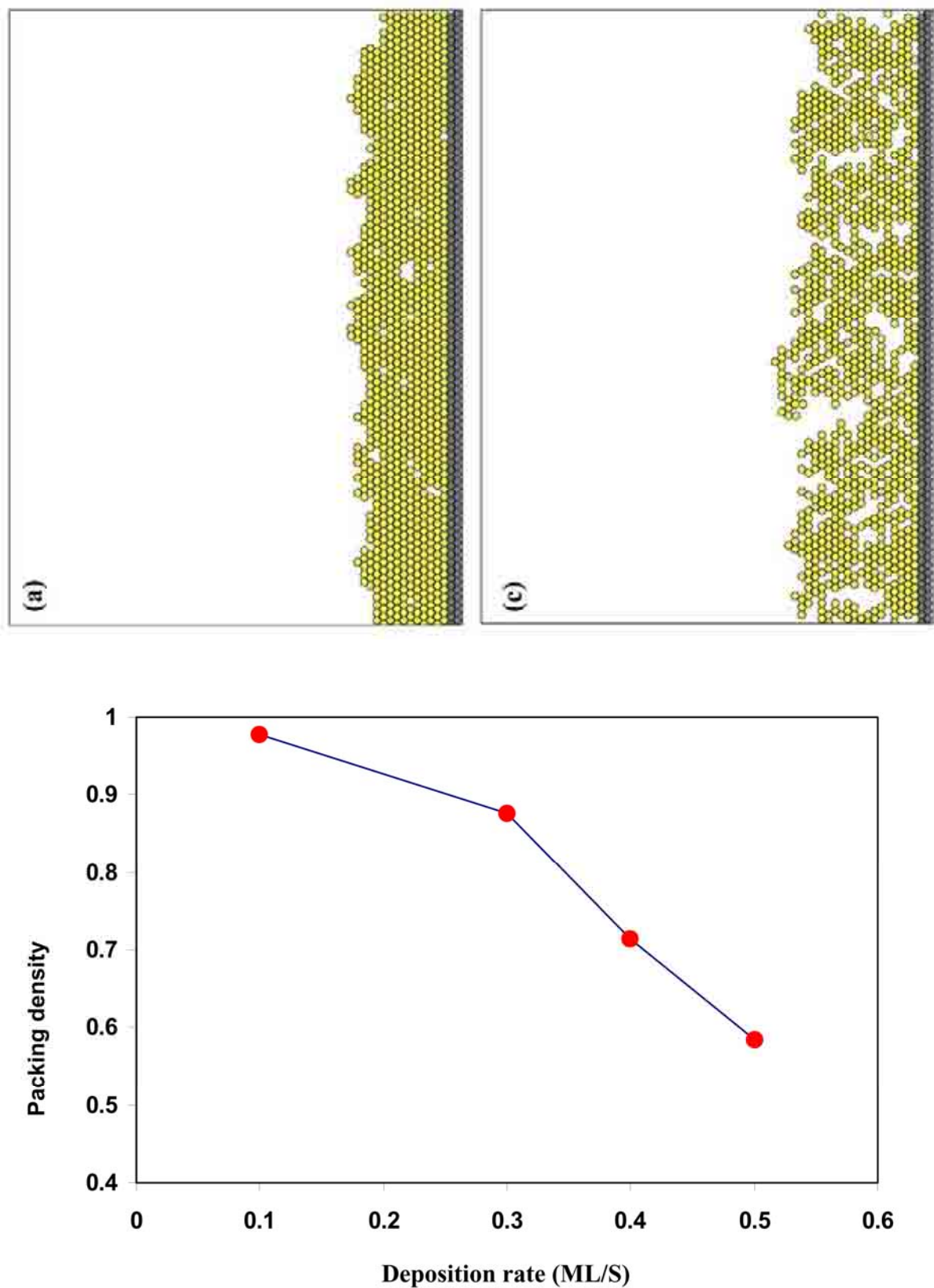
Figure 3. Thin film Growth on a smooth surface at T_s = 400 K, normal incidence and
for different deposition rates, R. a) R = 0.1 MLs^{-1}, b) R = 0.3 MLs^{-1},
c) R = 0.4 MLs^{-1}, d) R = 0.5 MLs^{-1}, e) packing density vs.
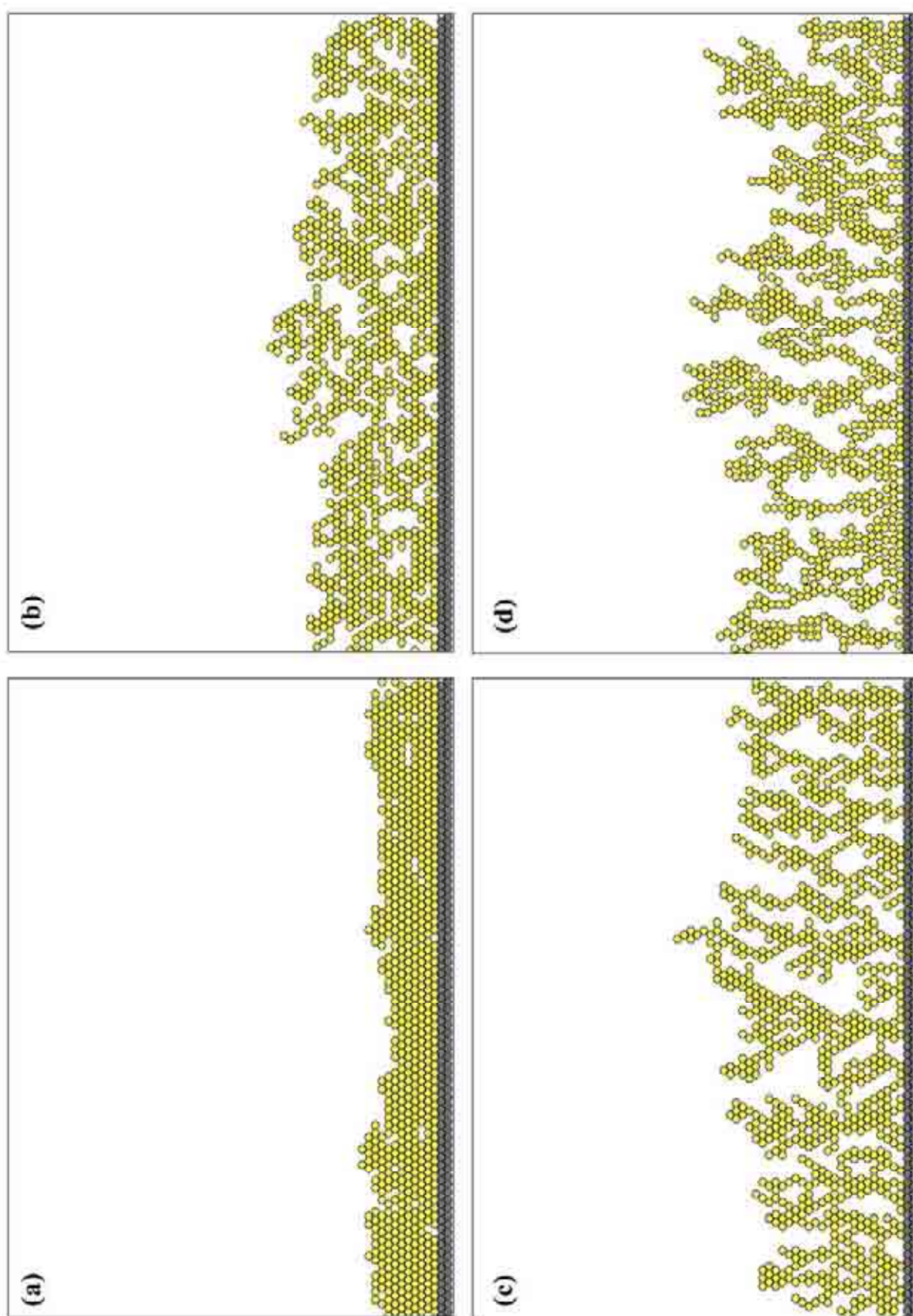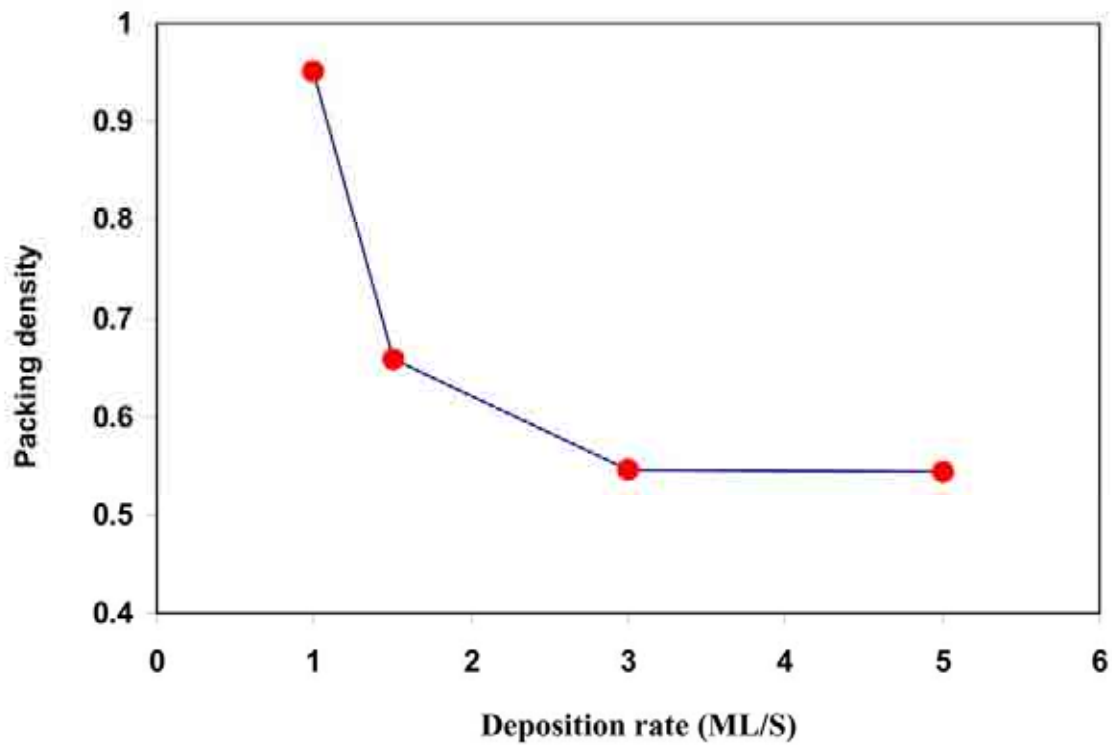
Figure 4. Thin film Growth on a smooth surface at T_s = 1000 K, normal incidence and for different deposition rates, R. a) R = 1 MLs^{-1}, b) R = 1.5 MLs^{-1}, c) R = 3 MLs^{-1}, d) R = 5 MLs^{-1}, e) packing density vs. deposition rate.
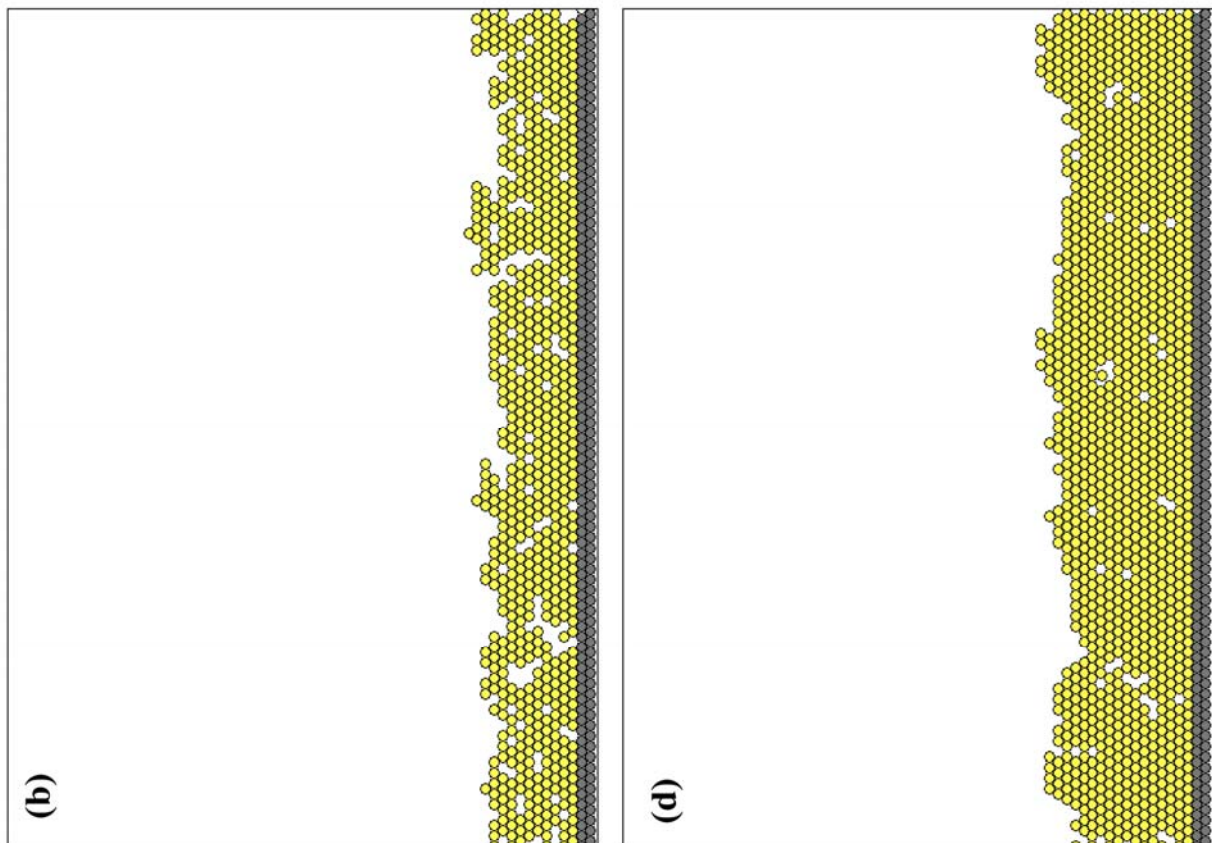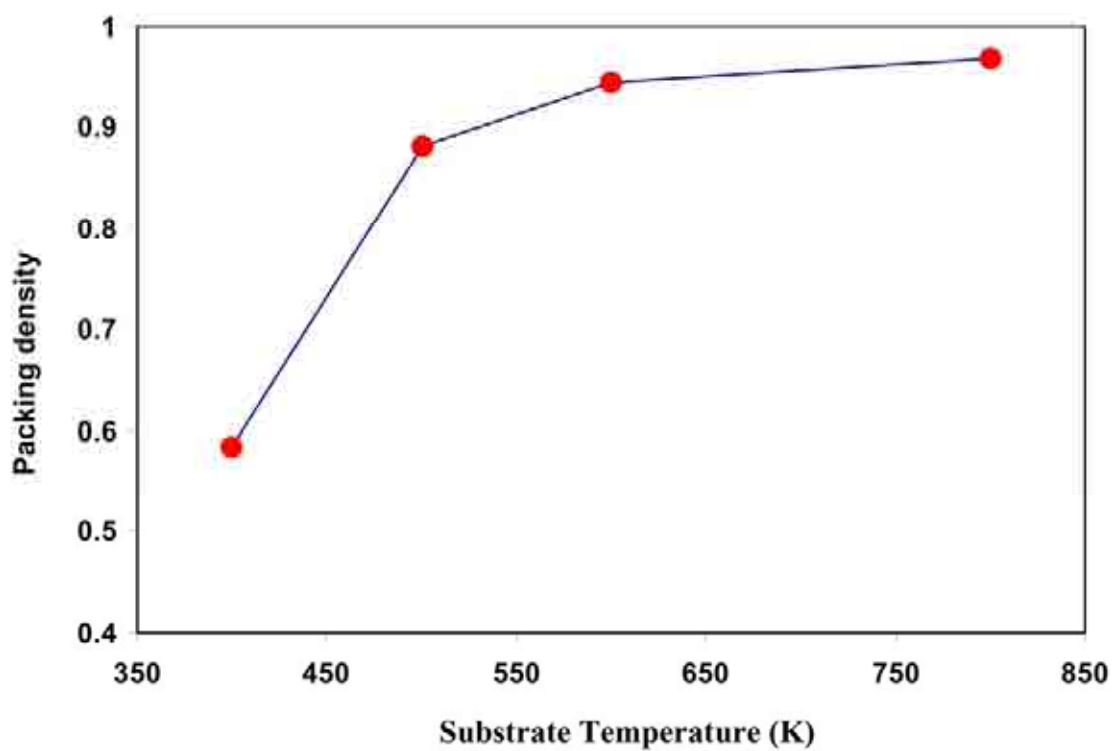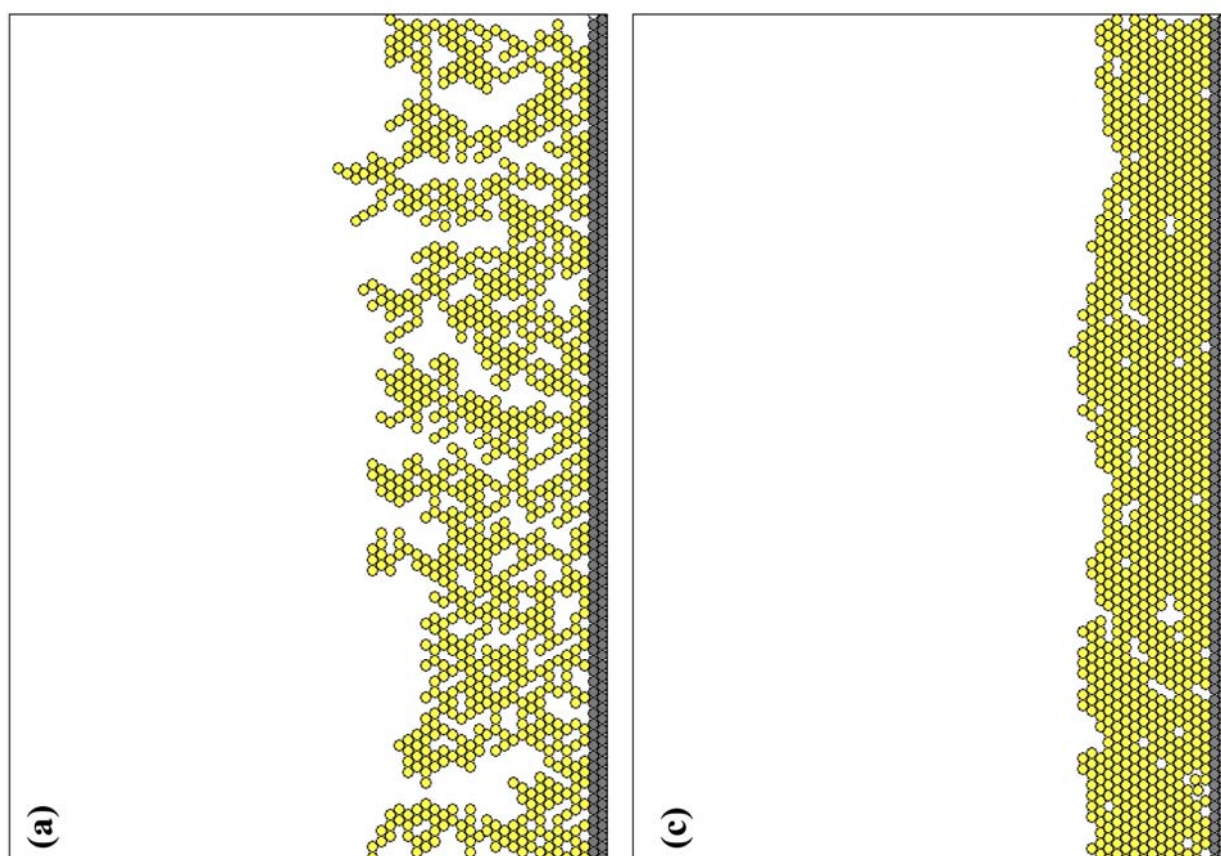
Figure 5. Thin film Growth on a smooth surface at normal incidence.
Deposition rate, R = 0.5 MLs^{-1}. a) T_s = 400 K, b) T_s = 500 K,
c) T_s = 500 K , d) T_s = 800 K, e) packing density vs. deposition rate.
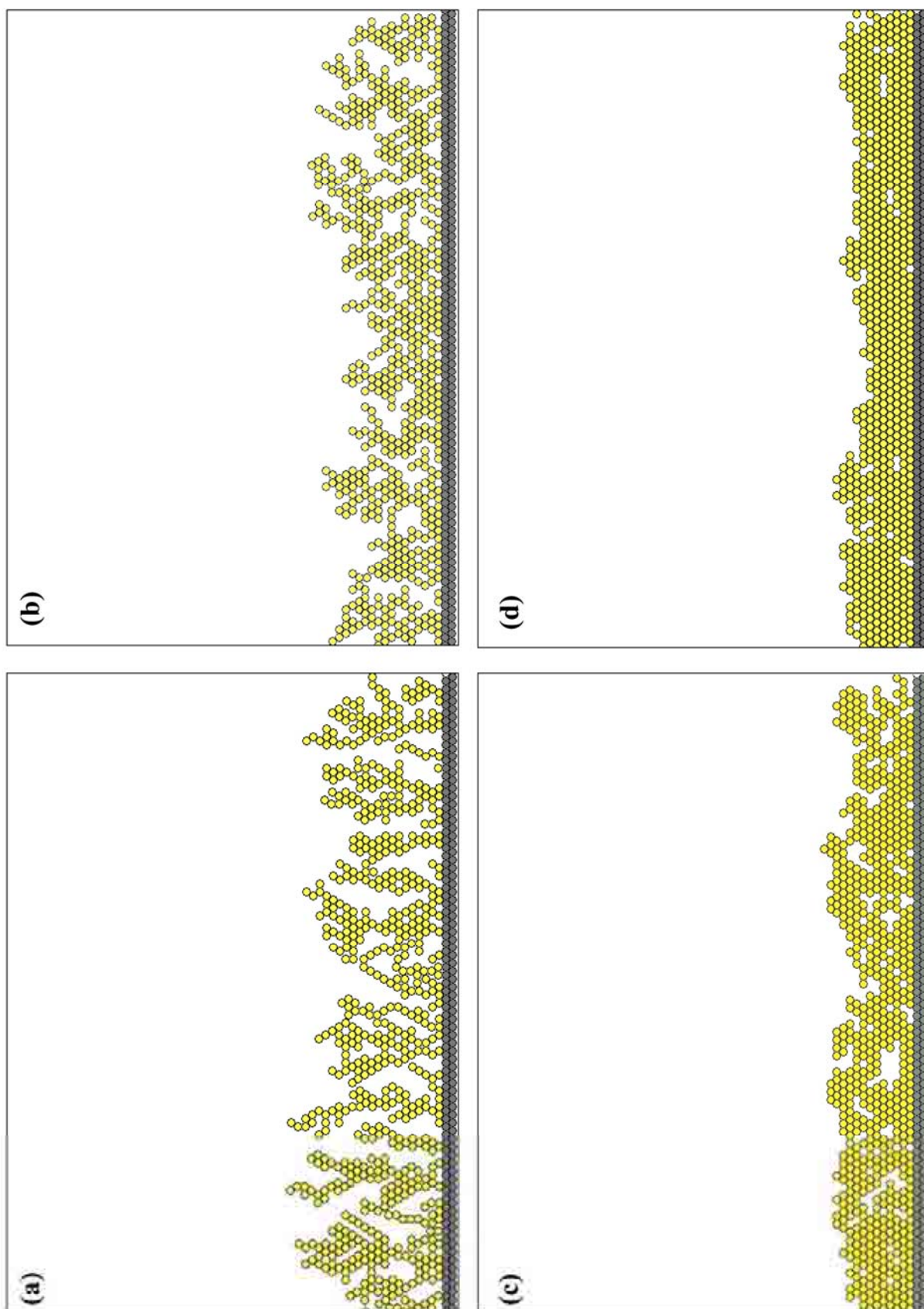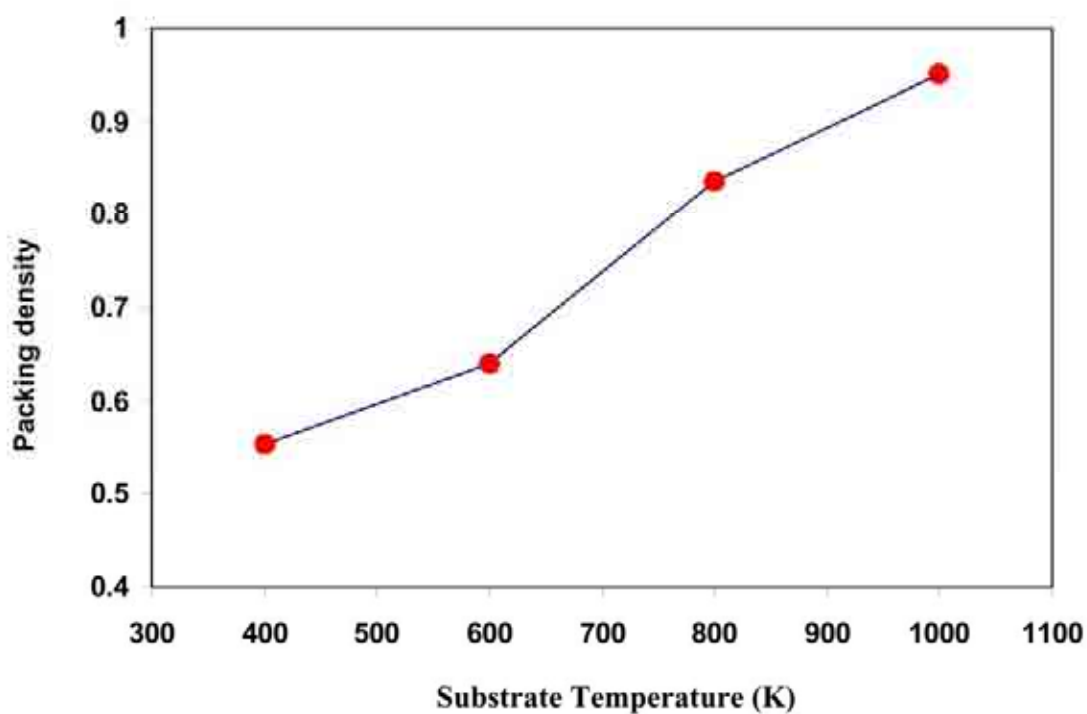
Figure 6. Figure 5. Thin film Growth on a smooth surface at normal incidence.
Deposition rate, R = 1 MLs-1 . a) Ts = 400 K, b) Ts = 600 K,
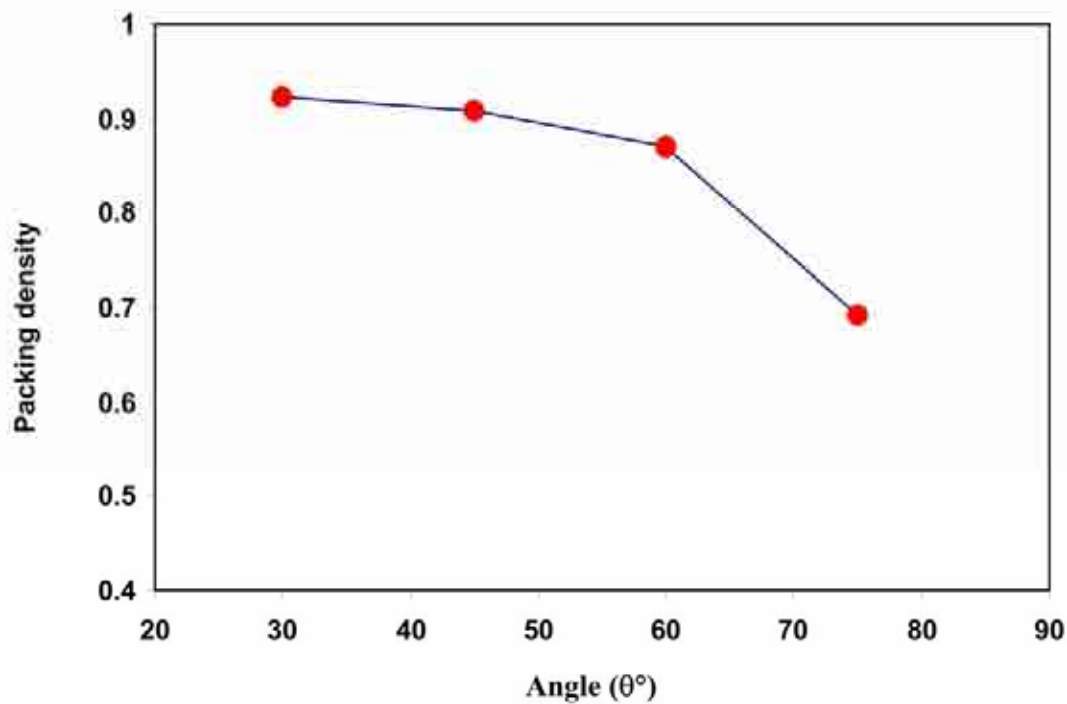c) Ts = 800 K , d) Ts = 1000 K, e) packing density vs. deposition rate.
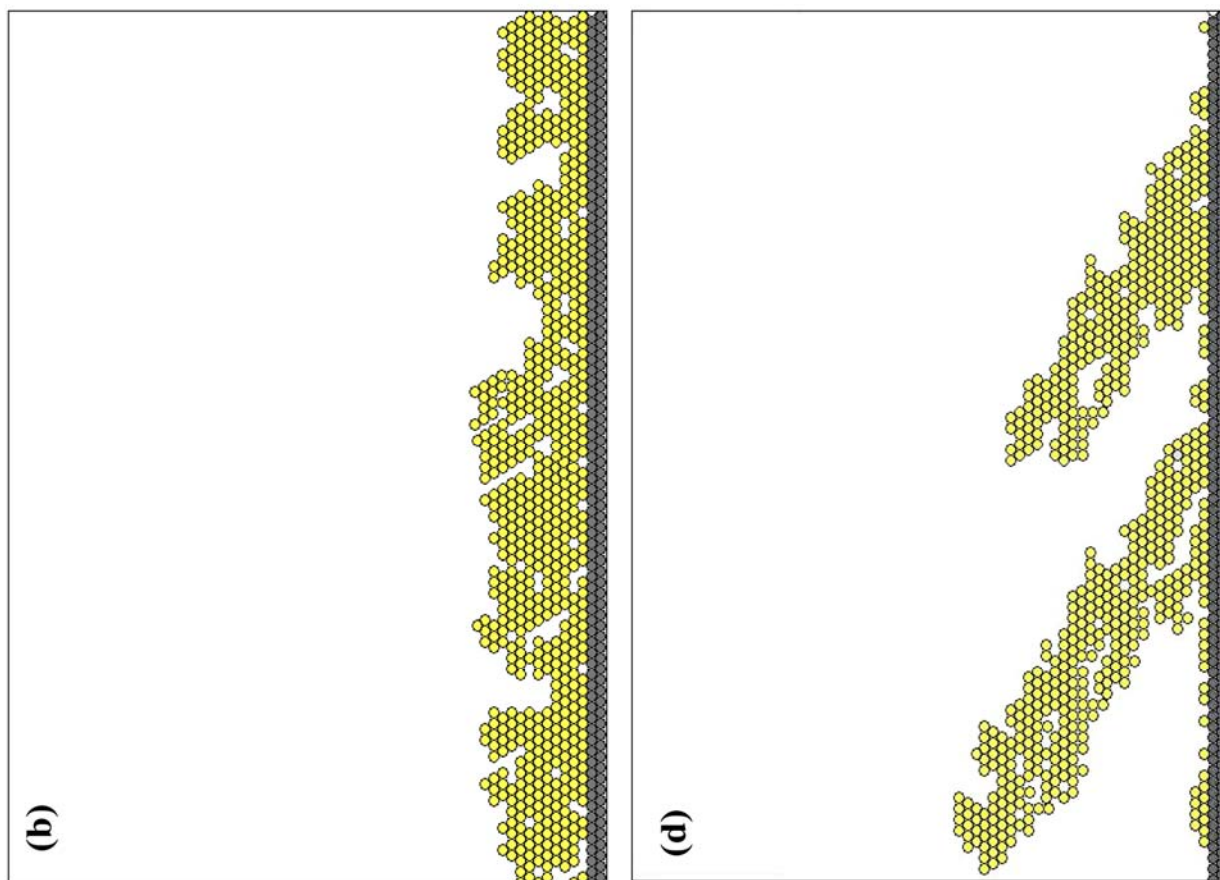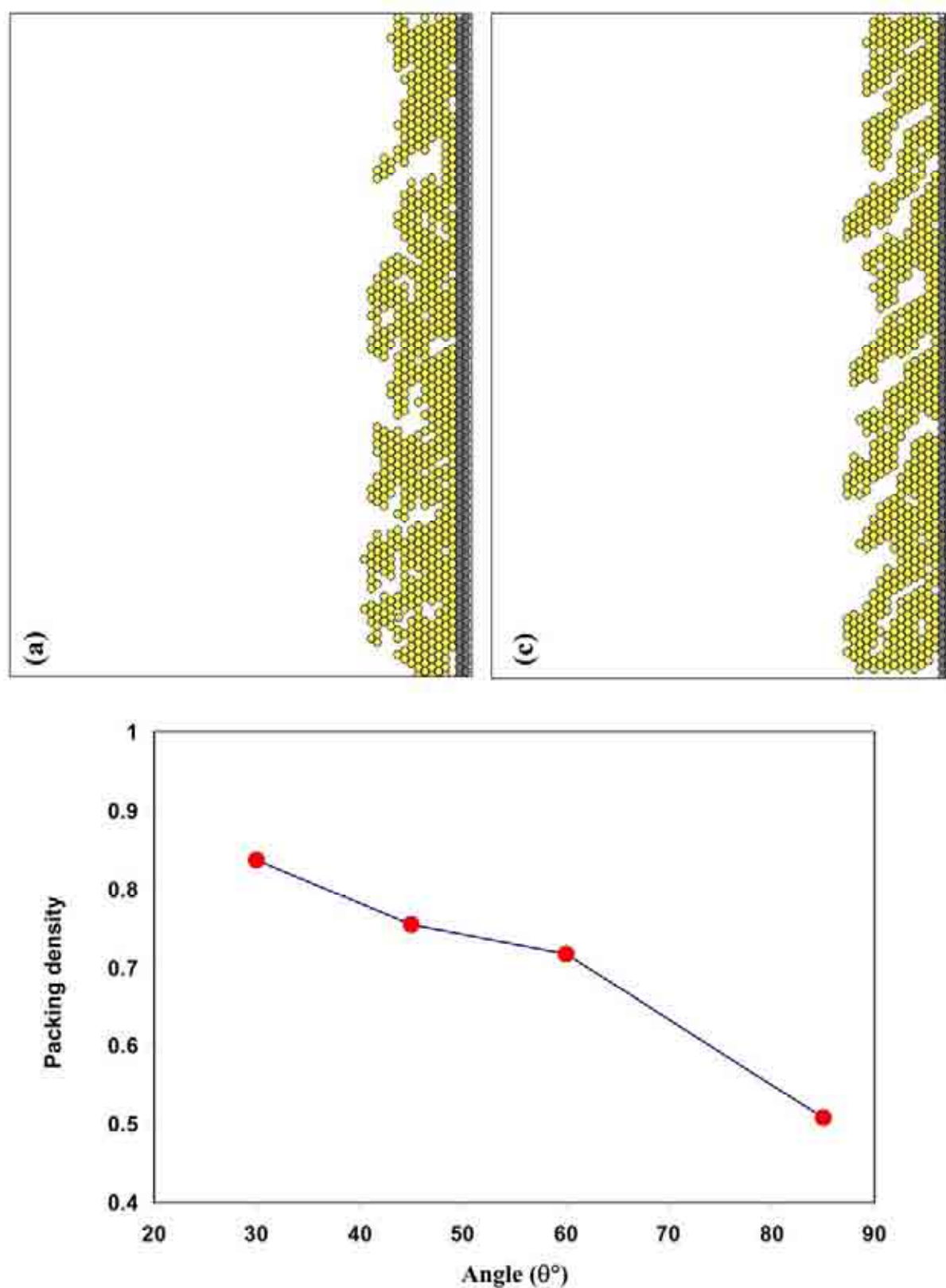
Figure 7. Thin film growth on a smooth surface at T_s = 400K, deposition
Rates of 0.3 MLs^{-1}, and for different angles of incidence. a) $\alpha = 30°$,
b) $\alpha = 45°$, c) $\alpha = 60°$, d) $\alpha = 70°$, e) packing density vs. deposition rate.

(b)

(d)

(a)

(c)
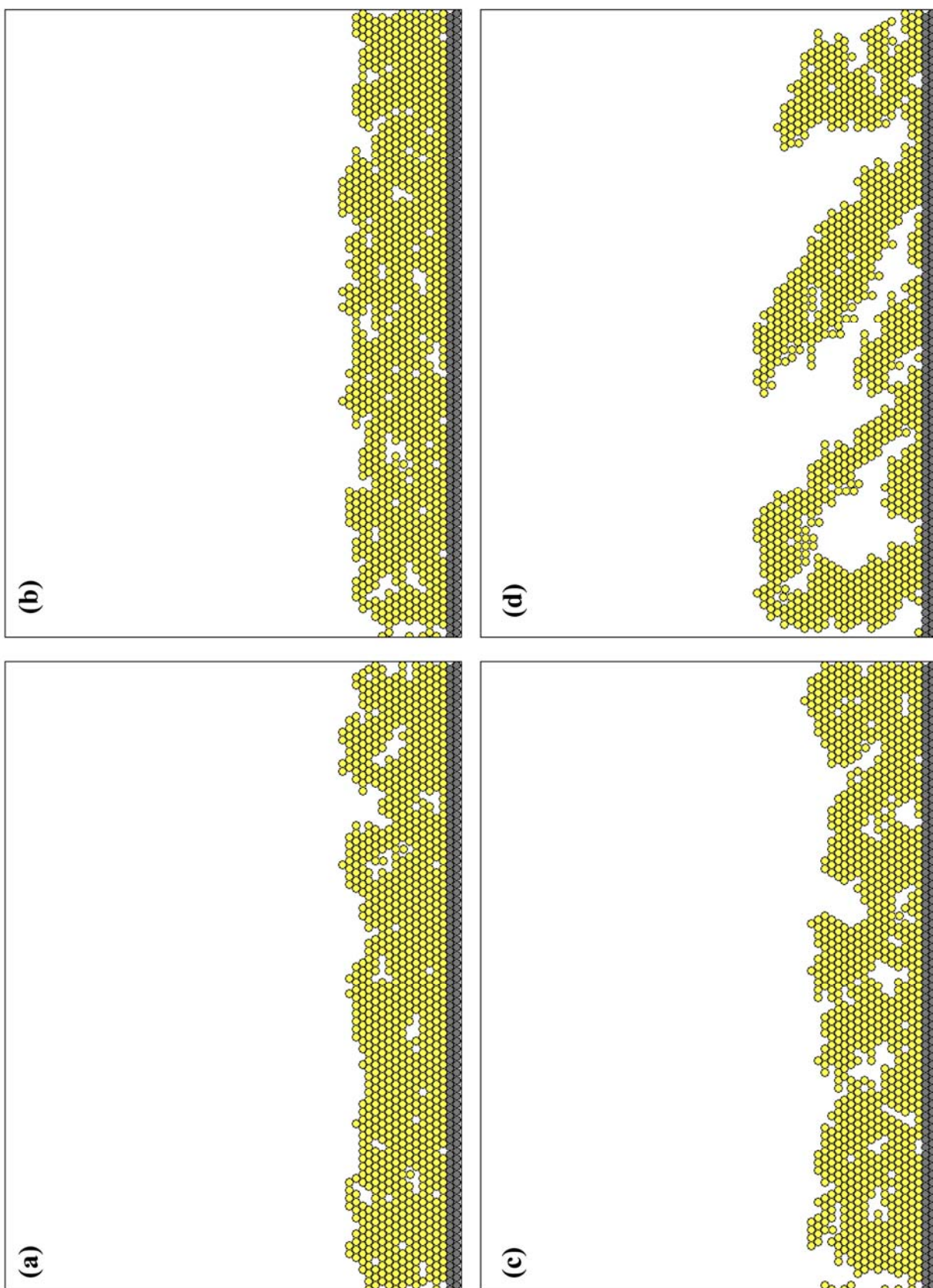
Figure 8. Thin film growth on a smooth surface at T_s = 600K, deposition
Rates of 0.5 MLs^{-1}, and for different angles of incidence. a) $\alpha = 30°$,
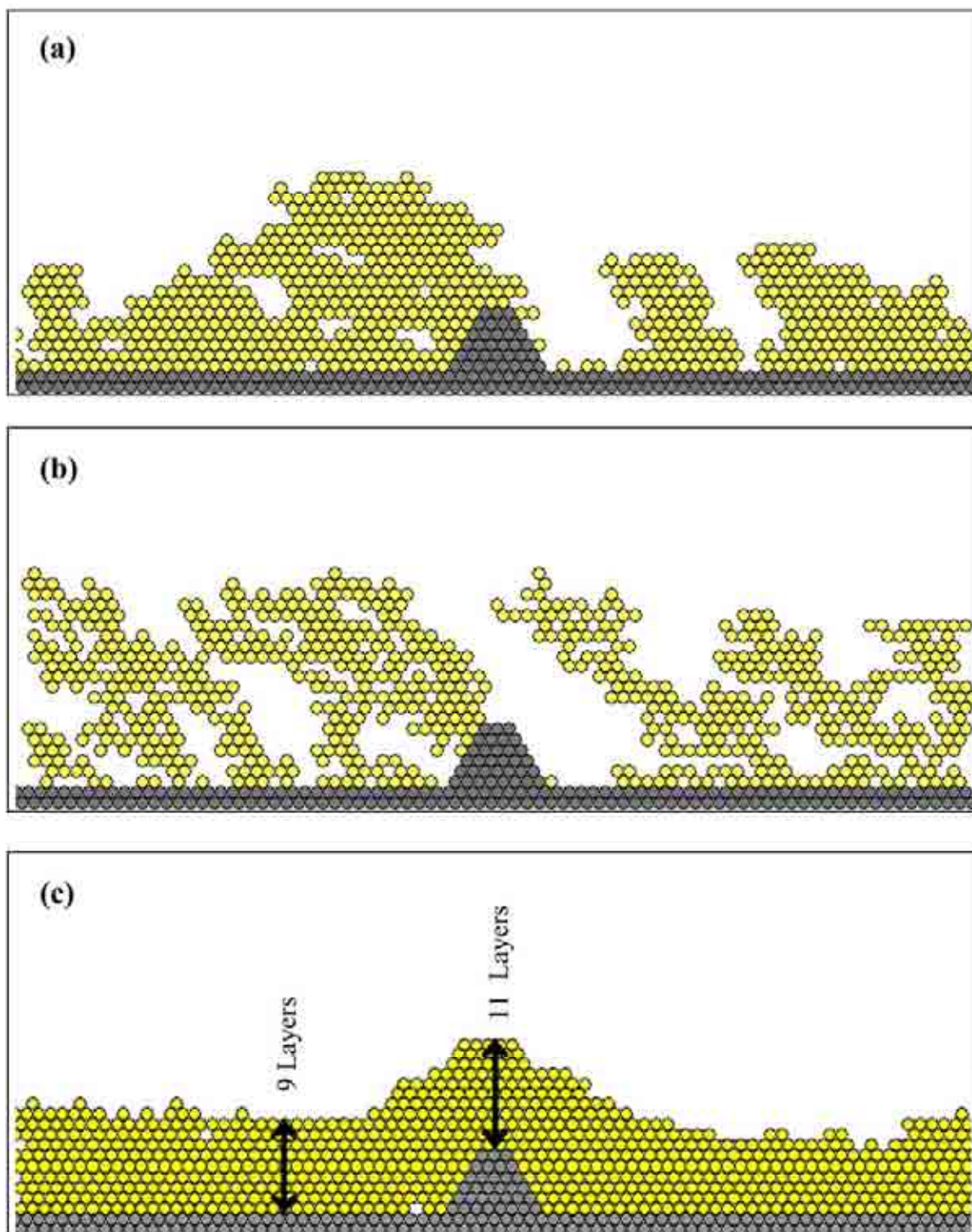b) $\alpha = 45°$, c) $\alpha = 60°$, d) $\alpha = 70°$, e) packing density vs. deposition rate.

Figure 9. Thin film growth on a surface with a peak. a) T_s = 800K, R = 0.5
MLs^{-1}, $\alpha = 60°$ b) T_s = 400K, R = 0.5 MLs^{-1}, $\alpha = 60°$ c) T_s = 1000K,
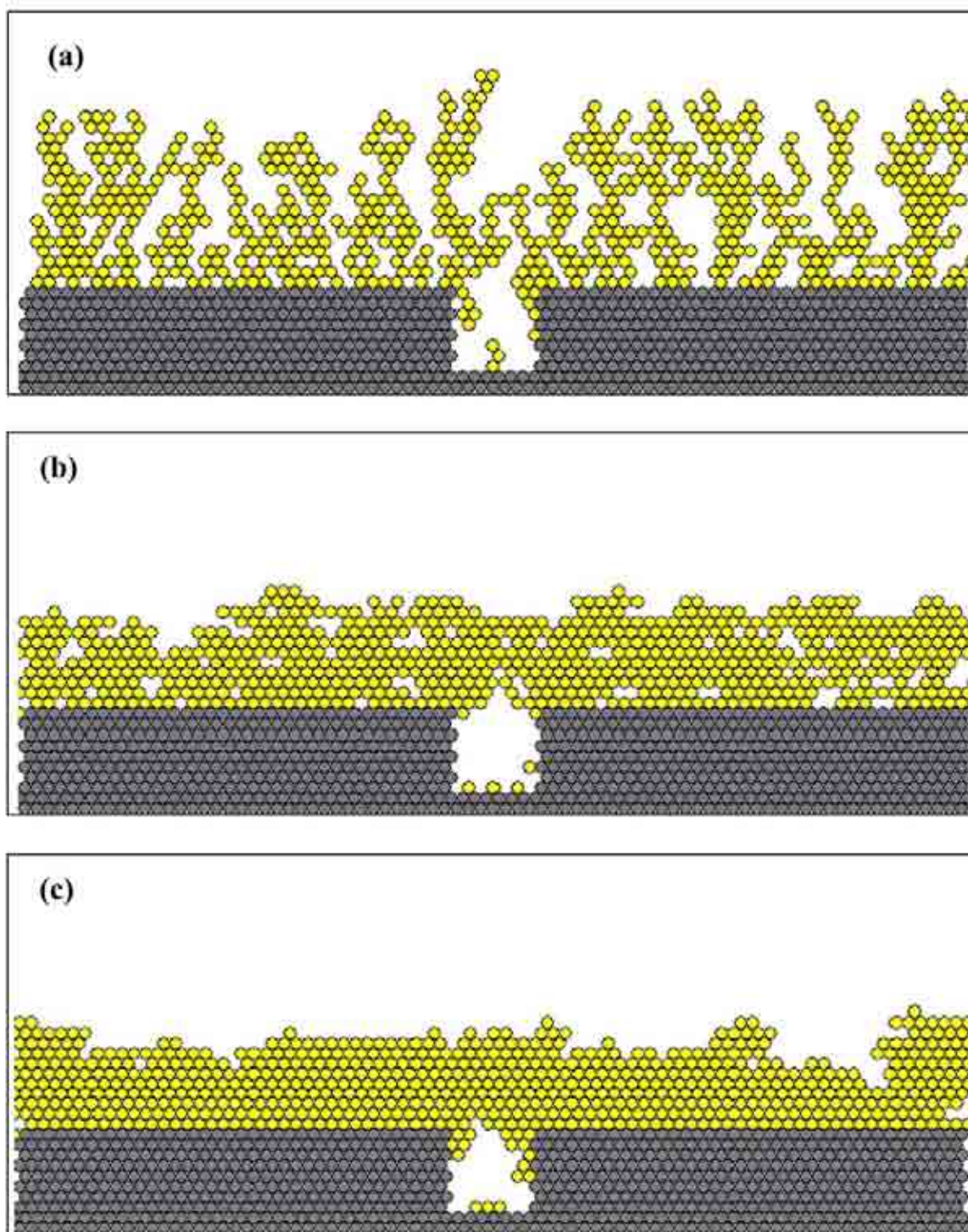R = 0.3 MLs^{-1}, $\alpha = 0°$.

Figure 10. Thin film growth on a surface with a trench at normal incidence.
a) $T_s = 400K$, $R = 0.7$ MLs^{-1}, b) $T_s = 400K$, $R = 0.3$ MLs^{-1},
c) $T_s = 800K$, $R = 0.3$ MLs^{-1}.

References

1- Dirks, A. G. and Leamy, H. J., *Thin Solid Films*, **47,** 219 (1977).

2- Messier, R., Giri, A. P. and Roy, R. A., *J. Vac. Sci. Technol,* **A2**(2), 500 (1984).

3- Grovenor, C. R. M., Hentzell, H. T. G. and Smith, D. A., *Acta Metall*, **32,** 773 (1984).

4- Savaloni, H., Gu, E., Player, M. A. and Marr, G. V., *Vacuum*, **43**, 965 (1992).

5- Barna, P. B. and Adamik, *Sience and Technology of Thin Films*, in F C Matacotta and G. Ottaviani, eds., World Scientific, Singapore, (1995) 1.

6- Savaloni, H. and Player, M. A., *Vacuum*, **46**, 167 (1995).

7- Savaloni, H. and Bagheri Najmi, S., *Vacuum*, **66**, 49 (2002).

8- Messier, R, Krishnaswamy, S. V., Gilbert, .L. R. and Swab, P., *J. Appl. Phys,* **51,** 1611 (1980).

9- Graighead, H. G., Howard, R. E., Sweeney, J. E. and Tennant, D. M., *J. Vac. Sci. Technol.,* **20,** 316 (1982).

10- Poulopoulos, P., Lindner, J., Farle, M. and Baberschke, K., *Surf. Sci.,* **437**, 277 (1999).

11- Kruhler, W., *Appl. Phys.* **A53**, 54 (1991).

12- Movchan,.B. A. and Demchishin, A. V., *Phys. Met. Metall.,* **28**, 83 (1969).

13- Thornton, J. A., *J. Vac. Sci. Technol.,* **12**, 830 (1979).

14- Messier, R., *J. Vac. Sci. Technol.,* **A4**, 490 (1986).

15- Kaiser, N., *Applied Optics*, **41**(16), 3053 (2002).

16- Hentzel, H. T. G., Grovenor, C. R. M. and Smith, D. A., *J. Vac. Sci. Technol.,* **A2**, 218 (1984).

17- Mazor, A., Srolovitz, D. J., Hagen, P. S. and Bukiet, B. G., *Phys. Rev. Letts.,* **60**, 424 (1989).

18- Mazor, A. and Srolovitz, *J. Vac. Sci. Technol.,* **A7**, 1386 (1988).

19- Player, M. A., Marr, G. V., Gu, E. and Savaloni, H., *J. Appl. Crystal.*, **25**, 770 (1992).

20- Bai, P., McDonald, J. F. and Lu, T. M., *J. Vac. Sci. Technol.*, **A9**, 2113 (1991).

21- Nakhodkin, N. G. and Shaldervan, A. I., *Thin Solid Films,* **10**, 109 (1972).

22- Messier, R. and Yehoda, J. E., *J. Appl. Phys.,* **58**, 3739 (1985).

23- Srolovitz, H., Mazor, A., Bukiet, B. G., *J. Vac. Sci. Technol.,* **A6**, 2371 (1988).

24- Bales, G. S. and Zangwill, A., *J. Vac. Sci. Technol.,* **A9**, 145 (1991).

25- Karunsasiri, R. P. U., Bruinsma, R. and Rudnick, J., *Phys. Rev. Letts.,* **62**, 788 (1989).

26- Srolovitz, D. J., *J. Vac. Sci. Technol.,* **A4**, 2925 (1986).

27- Muller, K. H., *J. Appl. Phys.,* **58**, 2573 (1985).

28- Muller, K. H, *J. Vac. Sci. Technol.,* **A3**, 2089 (1985).

29- Henderson, D., Brodsky, M. H. and Chaudari, P., *Appl. Phys. Lett.,* **25**, 641 (1974).

30- Das Sarma, S., Marmorkos, I. K. and Paik, S. M., *Surface Science,* **228**, 28 (1990).

31- Hrach, R. and Sobotka, M., *Int. Electronics,* **69(1)**, 49 (1990).

32- Muller Pfeifer, S., Van Kranenburg, H. and Lodder, C., *Thin Solid Films,* **213**, 143 (1992).

33- Leamy, H. J., Gilmer, G. H. and Dirks, A. G., *Current Topics Mater. Sci.,* **6**, 309 (1980).

34- Meakin, P., Ramanlal, P., Sander. L. M. and Ball, R. C., *Phys. Rev.,* **A34(6)**, 5091 (1986).

35- Jullien. R and Meakin. P, *Europhysics Letter,* **4(12)**, 1385 (1987).

36- Abelmane, L. and Lodder, C., *Thin Solid Films,* **305**, 1 (1997).

37- Nieuwenhuizen, J. M. and Haanstra, H. B., *Philips Technical Review,* **27**, 87 (1966).

38- Paudya, D. K., Rastogi, A. C. and Chopra, K. L., *J. Appl. Phys.,* **46**, 2966 (1975).

39- Meakin, P. B., *Phys. Rev.,* **A38**, 994 (1988).

40- Krug, J. and Meakin, P., *Phys. Rev.,* **A43 (2)**, 900 (1991).

41- Hara, K., Kamiya, M., Hashimoto, T., Okamoto, K. and Fujiwara, H., *J. Magn. Magn. Mater,* **73**, 161 (1988).